Mapping Lava Flows on Venus using SAR and InSAR: Hawai‘i Case Study

Authors: M.C. Brandin[1], D.T. Sandwell[1], C.L. Johnson[2,3], M.B. Russell[2]

[1] Institute for Geophysics & Planetary Physics

[2] Planetary Science Institute

[3] University of British Columbia Vancouver

Key Points:

- Under favorable mission and instrument conditions, InSAR can detect lava flows on Venus
- InSAR correlation effects from thermal subsidence can be seen for several months post-lava-flow-emplacement
- Lava flows are more easily visible in InSAR correlation maps than in differenced SAR amplitude maps

Abstract

We explore the potential for repeat-pass InSAR correlation to track volcanic activity on Venus' surface motivated by future SAR missions to Earth's sister planet. We use Hawai'i as a natural laboratory to test whether InSAR can detect lava flows assuming orbital and instrument parameters similar to that of a Venus mission. Hawai'i was chosen because lava flows are frequent, and well documented by the USGS, and because Hawai'i is a SAR supersite, where space agencies have offered open radar datasets for analysis. These data sets have different wavelengths (L, C, and X bands), bandwidths, polarizations, look angles, and a variety of orbital baselines, giving opportunity to assess the suitability of parameters for detecting lava flows. We analyze data from ALOS-2 (L-band), Sentinel-1 (C-band), and COSMO-SkyMed (X-band) spanning 2018 and 2022. We perform SAR amplitude and InSAR correlation analysis over temporal baselines and perpendicular baselines similar to those of a Venus mission. Fresh lava flows create a sharp, noticeable decrease in InSAR correlation that persists indefinitely for images spanning the event. The same lava flows are not always visible in the corresponding amplitude images. Moreover, noticeable decorrelation persists in image pairs acquired months after the events due to post-emplacement contraction of flows. Post-emplacement effects are hypothesized to last longer on the Venusian surface, increasing the likelihood of detecting Venus lava flows using InSAR. We argue for further focus on repeat-pass InSAR capabilities in upcoming Venus missions, to detect and quantify volcanic activity on Earth's hotter twin.

Plain Language Summary

Scientists are still unsure whether volcanic activity is presently occurring on Venus. Future missions to Venus may have the opportunity to detect new lava flows on Venus' surface using a process called interferometry, in which two radar images of a planet's surface over time are compared to see what's changed between them. Interferometry has been used to detect lava and volcanic activity on Earth in the past. We use Hawai'i as a natural laboratory, measuring lava flows there with interferometry, under simulated conditions of a Venus mission, to test whether it will be possible for future Venus missions to track lava flows with interferometry. From the results of our case study, we believe that future missions to Venus such as NASA's VERITAS will be able to do exactly that.

1 Introduction

Detection of present-day volcanic or tectonic activity on Venus would revolutionize our understanding of Earth's sister planet. On Earth, heat from planetary formation and that subsequently generated by radiogenic isotopes is primarily released to the surface by plate tectonics/recycling (~70% Turcotte, 1995) although hotspot volcanism and lithospheric conduction are also important (~30% Sleep, 1992). Venus and Earth have similar size, mass, location in the solar system, and by inference, composition, so Venus must also rid itself of excess heat by a combination of these three mechanisms (Solomon & Head, 1982). If the heat is lost primarily by conduction then the lithosphere should be ~40 km thick to sustain an average surface heat flow of ~74 mWm^{-2}. Topographic flexure (Johnson and Sandwell, 1994; Russell and Johnson, 2021; Smrekar et al., 2023) and gravity/topography (e.g., Anderson and Smrekar, 2006) studies suggest the thickness of the Venusian lithosphere is similar to that of Earth (> 80 km) so conduction cannot be the dominant mechanism. Venus has arcuate trenches similar in planform and cross section to subduction zones on the Earth (McKenzie et al., 1992) although there is little evidence for planet-wide plate tectonics (Byrne et al., 2021) and the overall length of inferred trenches on Venus is only about one third of the length of trenches on the Earth (Schubert and Sandwell, 1995). Other than the potential for highly efficient episodic tectonics, or cooling through lithospheric delamination (Turcotte, 1995) the remaining mechanism for heat loss is volcanism. On the Earth, there is near constant volcanic activity along the seafloor spreading ridges and on land volcanoes. Based on these arguments, one would expect Venus to have numerous active volcanoes. Indeed a recent study estimates the frequency of volcanic activity on Venus to be as high as 120 eruptions per Earth year (Byrne & Krishnamoorthy, 2022).

Synthetic Aperture Radar (SAR) images taken during NASA's Magellan mission (1989-1994) (Saunders et al., 1992) indicated that Venus has an extensive history of volcanism, and have enabled comprehensive mapping of lava flows, the ages of which are largely unknown (Head et al., 1992). The spatial crater density on the surface of Venus is low, and it is not possible to obtain statistically reliable relative regional surface ages (Campbell, 1999; Hauck et al., 1998; Phillips et al., 1992). Based on the low number, area, and density of impact craters, estimates for the average global surface age range from 300 Ma to ~1 Ga (McKinnon & Zahnle, 1997; Phillips et al., 1992; Schaber et al., 1992). Analysis of Magellan radar emissivity data, showing variations spatially correlated with individual features on the ground, suggests the youngest flows on Maat Mons are younger than 60 million years old, and perhaps as young as 9 million years old (Brossier et al., 2021). There is also circumstantial evidence for even more recent volcanism on Venus. Thermal emissivity anomalies detected by ESA's Venus Express Mission could result from lava flows younger than 250,000 years old (Smrekar et al., 2010), and these anomalies have been used to map the location and extent of younger vs older lava flows (D'Incecco et al., 2016). The Venus Monitoring Camera (VMC) aboard Venus Express also detected local fluctuations in surface temperature on a time scale of days to months, located along the Ganiki Chasma rift zone, suggesting the presence of volcanic activity related to the rift (Shalygin et al., 2015). Atmospheric evidence also suggests the presence of recent volcanism, such as the episodic injection of sulfur dioxide (Esposito, 1984). Recent comparisons of two Magellan SAR images of Atla Regio suggest that a volcanic event occurred in the 8-month gap between acquisitions (Herrick & Hensley, 2023). These observations indicate a volcanic vent increasing 4 km^2 in area, the first direct indication of volcanic activity on the Venusian surface. Still, the exact age of Venus' lava flows and the frequency with which they are emplaced now or in the past remains a mystery.

Detection of present and past volcanism is a major goal of upcoming SAR missions to Venus, namely NASA's VERITAS mission (X-band, Smrekar et al., 2022) and ESA's EnVision mission (S-band, Ghail et al., 2017). These may have the capabilities to detect volcanism within the mission lifetime using repeated SAR imagery amplitude and possibly SAR Interferometry (InSAR) (Meyer & Sandwell, 2012).

The primary focus of the Magellan mission was on imaging and mapping Venus using SAR, but not InSAR, as the use of amplitude and phase data for InSAR at Earth was first tested only around the time of the Magellan mission (Massonnet et al., 1993), and the orbital characteristics of the Magellan mission, as with most planetary missions, were not optimal for doing so. Measuring changes in radar backscatter amplitude has been used to accurately detect lava flows in previous terrestrial studies, including on the island of Hawai‘i (Poland, 2022; Dualeh, 2022). However, only using radar backscatter amplitude differences to identify lava flows has many challenges. Radar backscatter is most sensitive to the roughness of the surface at the wavelength of the radar - fresh lava flows can therefore prove difficult to map, disappearing in the radar image where their flow becomes smooth, and reappearing in a’a or pahoehoe-textured areas (Herrick et al., 2023). Although very large changes in the shape of the surface can be seen in radar backscatter amplitude changes, such as those found by Herrick & Hensley (2023), smaller, or relatively flat lava flows are difficult to detect. In short, if the surface texture remains roughly the same before and after a lava flow is emplaced, it may go undetected.

Previous studies show InSAR is very effective for mapping lava flows (Zebker et al., 1996; Lu et al., 2000; Rowland et al., 2003; Diettrich et al., 2012; Poland, 2022), and can be used when changes cannot be distinguished in radar backscatter. InSAR measures surface change by comparing radar phase between two co-registered SAR scenes collected at different times. Where the surface scatterers have not changed orientation with respect to the satellite view between two images, coherence will be high, but where the surface has changed in the time between acquisitions, coherence will be low. The phase can be computed at a single pixel but the coherence requires averaging or filtering over an area of several pixels. The coherence will remain high as long as the phase variations are relatively uniform within the averaging area. We smooth the coherence with a Gaussian filter having 0.5 gain filter at 75 m half wavelength, which is comparable to a 36 m boxcar filter, a commonly used length scale for multilook averaging (Zebker & Villasenor, 1992). Moreover, the phase of the overall interferogram can be highly distorted by atmospheric phase delays while the corresponding coherence image will be largely insensitive to the atmospheric distortions and more sensitive to changes in the surface scatterers. This coherence is measured with a value from 0 to 1 referred to as correlation (Zebker & Villasenor, 1992). On Earth, decorrelation between two SAR images of the same area is often caused by water and vegetation, which causes surface changes between SAR scenes (Zebker & Villasenor, 1992). Variations in the position of the satellite also affect correlation, and the larger the distance between the satellite positions at different acquisition times, known as the "physical perpendicular baseline," the lower the overall correlation and its maximum possible value (Gatelli et al., 1994). The length of time between acquisitions, or "temporal baseline," also lowers correlation, because of small surface changes accumulating over time (Lu & Freymueller, 1998).

New lava flows cause substantial decorrelation of SAR images by repaving the surface, completely changing the ground's scattering properties between images collected before and after flow emplacement. However, once a flow becomes inactive, and the lava completely cools and subsides, its surface remains stable between image acquisitions, yielding high correlation in subsequent acquisitions, at least in arid regions (Diettrich et al., 2012). It is this effect that makes InSAR correlation useful in lava flow mapping, as new, active lava flows will exhibit very low correlation compared to old, inactive lava flows around them (Figure 1).

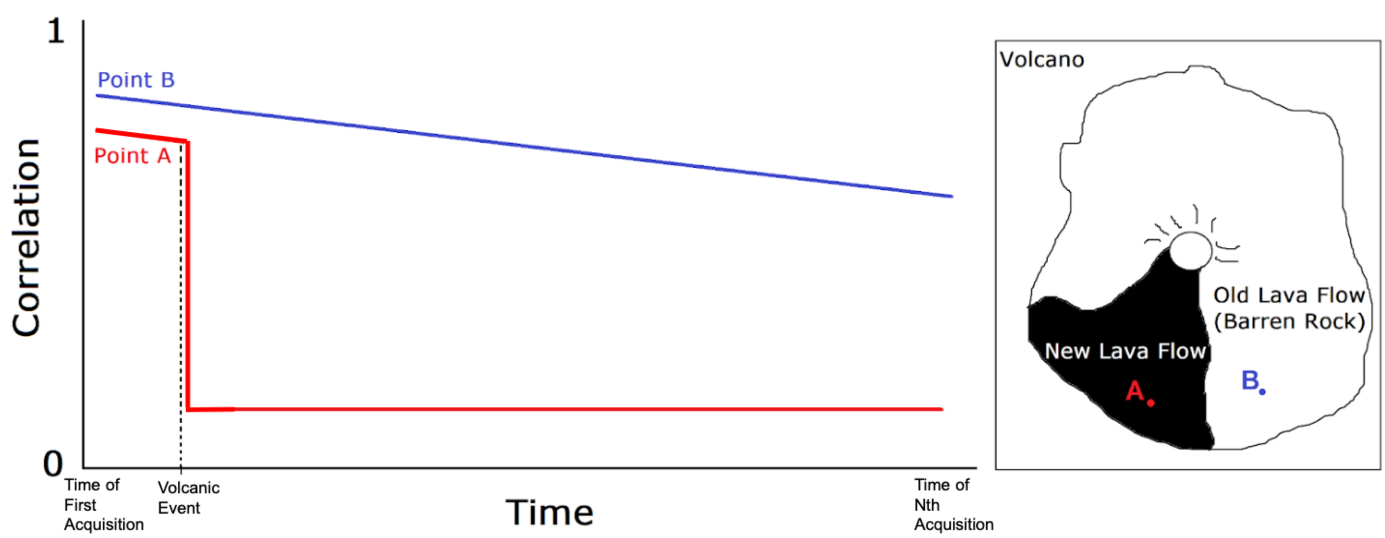

Figure 1. Schematic of the correlation of InSAR image pairs over active and inactive volcanic flows. The InSAR correlation of an active lava flow area of an image taken before the eruption with all following images will drop dramatically after the event, and stay low for any interferogram made between the first, pre-eruption acquisition and any acquisition taken after the volcanic event, no matter the length of time that has transpired. In contrast, for inactive lava flow

areas, the InSAR correlation will initially be high but decrease steadily with time in subsequent interferograms due to small, accumulating changes in the surface scatterers (Lu & Freymueller, 1998).

Venus provides unique challenges for an InSAR mission; physical perpendicular baselines may be large because of the highly eccentric orbits common to planetary missions. Furthermore, Venus' slow rotational period means that the matching tracks (descending or ascending) of an orbiting satellite only passes over the same location once every 243 days, constraining the temporal baseline, and limiting the total number of repeat passes over the mission lifetime to ~5 at best (Meyer & Sandwell, 2012). Despite these challenges, NASA plans to utilize InSAR on VERITAS (Smrekar et al., 2022), and there was initially discussion of using InSAR on EnVision (Ghail et al., 2017). Although InSAR is no longer a planned mission activity for EnVision (ESA/SCI, 2021) because no near repeat orbits are planned (ESA/SCI, 2023), repeat orbits with short interferometric baselines may occur, especially at high latitudes where the orbital tracks converge. In this study, we aim to inform potential future Venus InSAR efforts to detect lava flows by exploring the most effective radar bands, orbits, temporal baselines, and analysis tools.

We use the Island of Hawaiʻi as a natural laboratory for the following reasons: 1. It is heavily studied, including other InSAR lava flow tracking experiments (Zebker et al., 1996; Mouginis-Mark, 2004; Diettrich et al., 2012; Poland, 2022); 2. it is an open data supersite; and 3. it is a volcanically active area with new lava flows frequently covering older emplaced flows. To investigate the optimal methods for lava flow detection with InSAR, we use data from three satellites, namely Sentinel-1 operating at C-Band (5.6 cm), ALOS-2 operating at L-Band (23.6 cm), and COSMO-SkyMed operating at X-band (3.1 cm). These satellites travel in orbits having near-exact repeats, so interferometry is commonly possible. We employ two methods, InSAR correlation and SAR amplitude, to investigate and monitor lava flows from two separate eruptions (Figure 2).

2 Methods

We consider two main eruption phases on the island of Hawai‘i to characterize changes in SAR amplitude and correlation. The 2018 eruption has the best temporal coverage, especially at C-band. This enables us to compare amplitude and coherence changes before, during and long after the eruption. The 2022 eruption at the summit of Mauna Loa provides excellent spatial mapping of amplitude and coherence in L, C, and X-band.

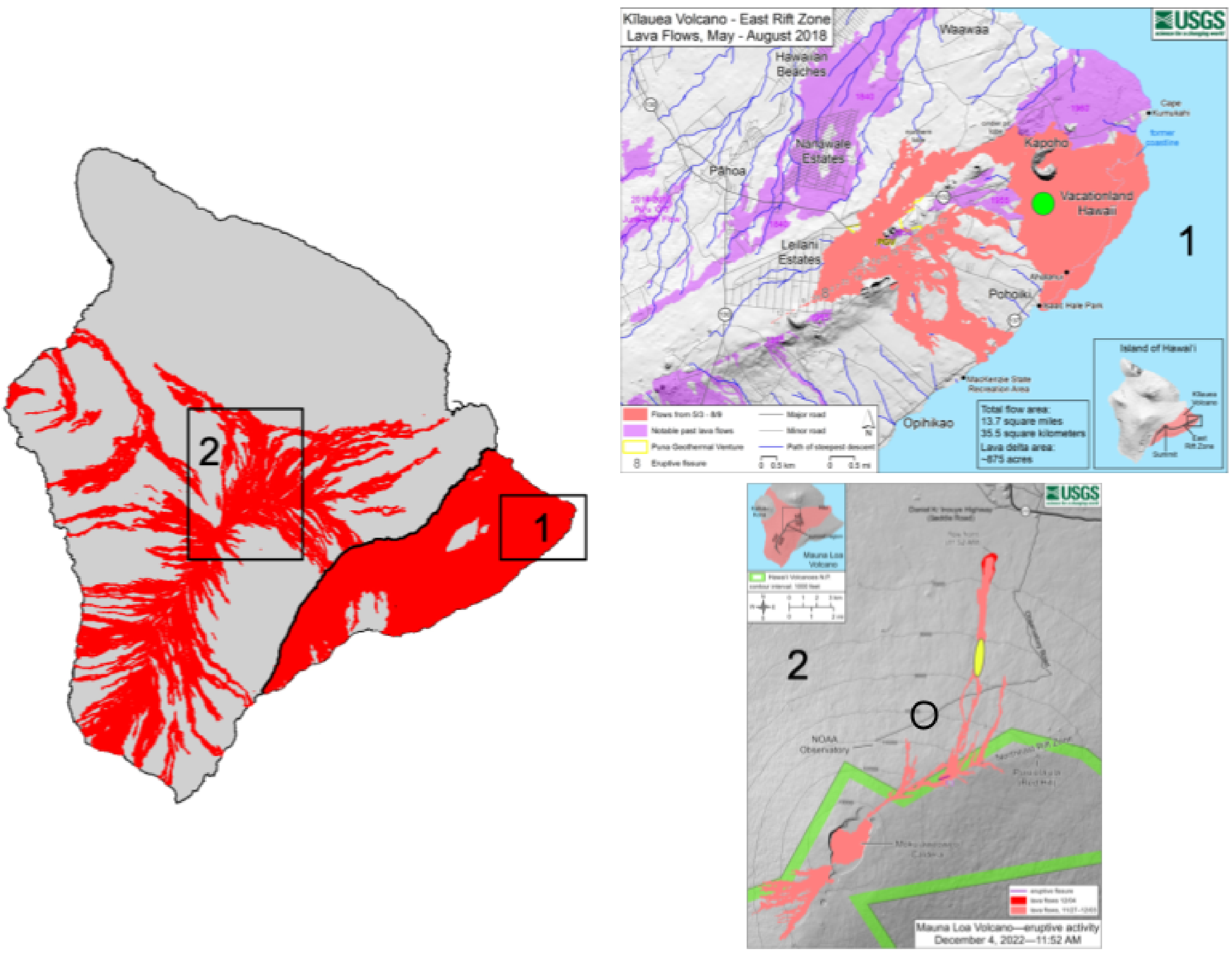

Figure 2. Location and extent of the two lava flows analyzed in this paper. Left: USGS map of Hawai‘i showing all lava flows in the past 1000 years in red (USGS). Boxes 1 and 2 show the approximate extents of the USGS maps for the 2018 and 2022 events shown in Top Right and Bottom Right respectively. Top Right: USGS map of the 2018 Kīlauea Lower East Rift Zone eruption final extent (USGS, 2018). Purple shows old emplaced lava flows, pink shows the 2018 flow, and overlaid green oval marks the general location from which SAR amplitude and InSAR correlation values were sampled over the new lava flow. Bottom Right: Published USGS map of

the 2022 Mauna Loa lava flow, showing extent by December 12, 2022, in pink and red (USGS, 2022). Overlaid yellow oval marks the general location of the area from which SAR amplitude and InSAR correlation values were sampled. Overlaid black ring marks the general location from which values were sampled over the older, inactive surface.

2.1 C-band analysis of the 2018 eruption

To study the May 2018 Kīlauea Lower East Rift Zone Eruption (Neal et al., 2019; Patrick et al., 2019; Dietterich et al., 2021), we assembled more than 200 Sentinel-1 (C-band) SAR images from both A and B satellites for times when both were operational, with a 6 to 12 day repeat pass period over the Island of Hawaiʻi spanning March 2018 to December 2021. We used only data from a descending orbit (track 87). Using the software GMTSAR (Sandwell et al., 2016), we processed all possible 20,000+ combinations of InSAR image pairs. We used a Gaussian filter with a 0.5 gain at a wavelength of 120 meters for multi-look averaging amplitude, phase, and coherence, and used the Shuttle Radar Topography Mission (SRTM1) 30 m data for our digital elevation model (DEM) to remove the topographic phase (Farr et al., 2007).

Having assembled all InSAR pairs and calculated phase differences, radar amplitude differences, and correlation, we then computed the average correlation for specific regions of interest on the map for each pair. Our two main regions of interest were 1. “active lava flow areas,” consisting of an old lava flow or bare ground that was largely covered by new lava during the eruption event, contrasted with 2. “inactive lava flow areas,” consisting of old lava flow or bare ground that was completely untouched by new lava flows for the entire duration of the data set, as sketched in Figure 1. The locations of all “active” and “inactive” areas sampled are shown in Figure 2.

For the 2018 eruption, our active lava flow area is the old 1955 lava flow and parts of the 1960 flow, which were largely devoid of vegetation before the eruption and completely covered by new lava during the event (Figure 2). The presence of extensive vegetation in this area made analysis difficult, as only small areas could be sampled and studied. Our inactive lava flow area was an unvegetated slope of Mauna Loa, which had no new lava flows during this time period

(2018-2021).

For each pair of SAR images, we also computed the relative change in SAR amplitude between the two images, by taking the absolute difference between them and dividing by their average to normalize to 1. In the same way we sampled average correlation, we sampled the average amplitude difference of each image pair, for both the active and inactive lava flow areas. No radiometric or other corrections were performed on the amplitude data beforehand.

2.2 L, C, and X-band spatial and temporal analysis of the 2022 Mauna Loa eruption

The November-December 2022 eruption of Mauna Loa (Figure 2) provided an opportunity to explore the strengths and weaknesses of imaging an eruption using three radar wavelengths L, C, and X-band. There is little water or vegetation on the slopes of Mauna Loa, so the inherent correlation of the old emplaced flows is very high at all three radar wavelengths, similar to conditions expected on Venus, making this eruption an ideal case study for our method. As discussed above, the orbits of the reference and repeat images must be within the critical baseline to recover interferometric phase and coherence. The critical baseline (Zebker and Villasenor, 1992) is given as

EQUATION 1: $b_{crit} = (\lambda r) / (2R\cos^2\theta)$

where c is the speed of light, r is the slant range (~600 km), θ is the look angle (~20-45 degrees), λ is the wavelength, and R is the pulse length = 1/bandwidth. The maximum coherence of an interferogram is

EQUATION 2: $\gamma = 1 - (b_{perp}/b_{crit})$

where b_{perp} is the range-perpendicular distance in space between the reference and repeat orbits. For similar orbital geometry, the main factors controlling the critical baseline are the radar bandwidth and the radar wavelength. The radar wavelengths of L, C, and X-band are 30-15 cm, 7.5-3.75 cm, and 3.75-3.5 cm, respectively, so all else being equal, the critical baseline for L-band will be 4 times longer than C-band and 8 times longer than X-band.

At L-band, the 2022 eruption site was imaged only 6 times with JAXA's ALOS-2 spanning June 2022 to July 2023. From this limited set, we generated 15 interferograms spanning the eruption and lava flow event. The perpendicular baseline of all the interferograms was well within the critical baseline of ~6.5 km.

At C-band the 2022 eruption site was imaged 23 times by Sentinel-1 spanning October 2022 to June 2023. Because of the relatively short perpendicular baselines, we processed 162 InSAR pairs. Once again, we calculated and sampled the average correlation and average amplitude difference at an active and inactive lava flow area for each InSAR pair.

At X-band we assembled 10 images from ASI's COSMO-SkyMed, spanning October 2022 to April 2023. Each sequential image pair had a temporal spacing of around 15 days. Unfortunately, the repeat orbits of COSMO-SkyMed (CSK) are not normally controlled within the relatively small critical interferometric baseline of around 1.3 km, so only a fraction of the interferograms are usable. Many have maximum correlation far less than 1, so the correlation contrast can be low. Of the 45 interferograms we processed, fewer than 15 had sufficiently high correlation to distinguish surface features, with many being completely decorrelated. Still, those well-correlated interferograms gave us an opportunity to compare interferograms of the 2022 eruption in all three bands, L, C, and X. This also gave us a unique opportunity to test the effects of high physical baselines on our detection method, as this will be a major hurdle of any Venus InSAR mission.

3 Results

3.1 Analysis of 2018 Eruption

Our schematic (Figure 1) for how new emplacement of lava flows would affect the correlation between InSAR image pairs is supported quantitatively by the Sentinel-1 data for the 2018 eruption, (Figure 3). The correlation of the inactive area stays high, slowly decreasing, on average, in a linear fashion over several years. The correlation of the active area however, drops substantially with the emplacement of new lava, and remains low more than a thousand days later. Substantial noise is present due to baseline effects, and because of the presence of some light vegetation and water in these areas, both of which cause rapid decorrelation in InSAR images, however, neither are present on the Venusian surface. All things being equal, a higher signal-to-noise ratio in such derived products might be expected from a Venus mission. Venus' atmosphere may cause significant variability in the strength of the coherence signal, leading to lower signal-to-noise overall (Meyer & Sandwell, 2012)

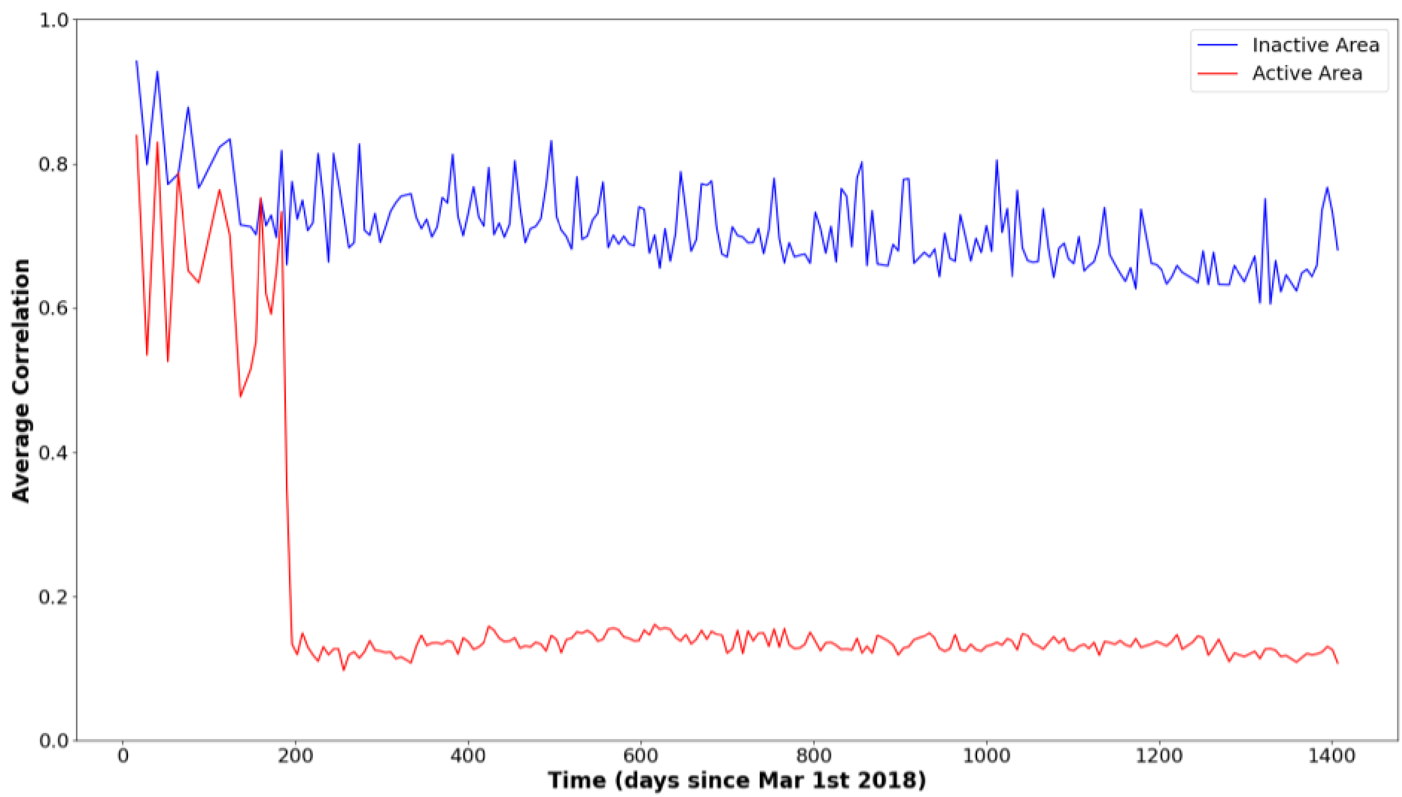

Figure 3. Average InSAR correlation over active (red) and inactive (blue) lava flow areas, between one image before the 2018 eruption (March 1st 2018) and every other image in the data set, showing the evolution in time of correlation in both areas. Lava emplacement occurred around day 190 (July 9th 2018). Time on the x-axis refers to the date of second acquisition.

The average correlations of all possible image pairs for both the active and inactive areas is shown in Figure 4. There are three distinct types of correlation in relation to the lava flow: 1. The inactive area (Figure 4, right) has no notable correlation changes between pairs. There are some bands of relatively lower correlation believed to be caused by rainfall, which can reduce correlation (Lohman & Bürgi, 2023); 2. All interferograms spanning the event have low correlation as seen in area B of Figure 4 left; 3. There is an interesting pattern in correlation for interferograms with both acquisitions after the event. The coherence between sequential SAR images does not immediately return to the high value of ~0.8 because the surface scatters of the lava flow are still in motion. This is due to cooling and settling of the lava which can take several years depending on thickness of the flow as noted in previous studies (Diettrich et al., 2012; Stevens et al., 2001). These post-emplacement signatures can also be seen in our results for the other eruption and are discussed in more detail in section 4.1.

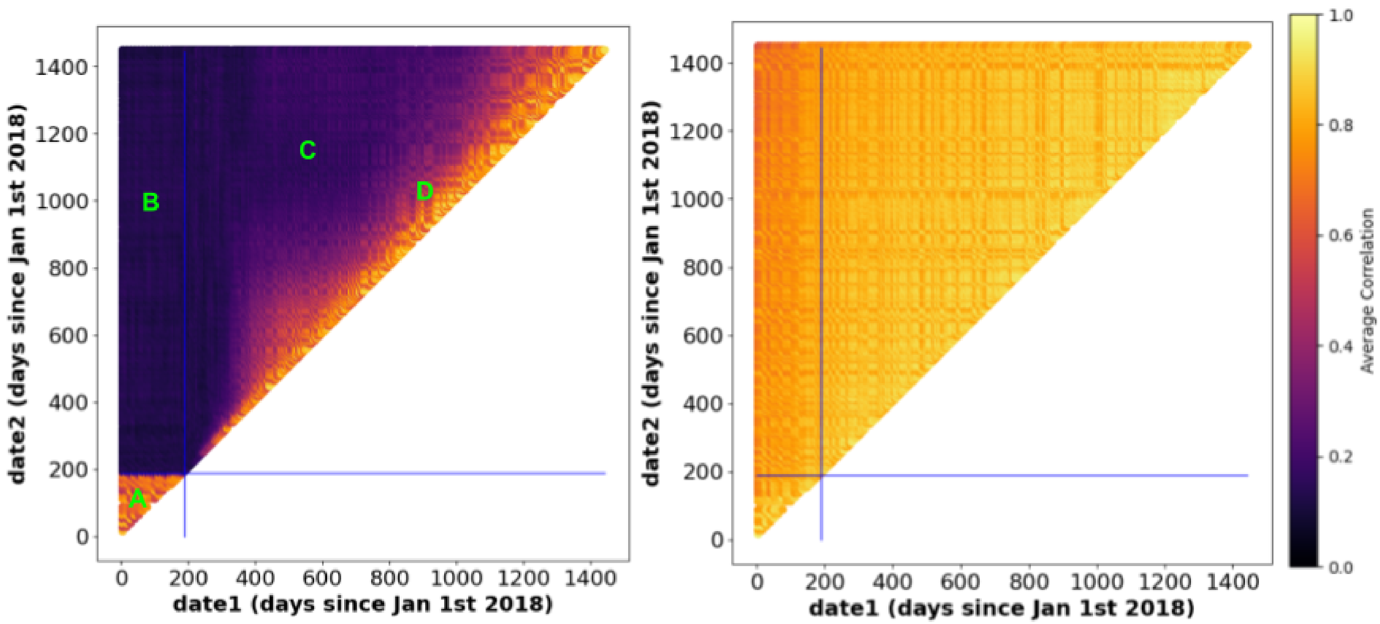

Figure 4. Plots of average correlation over specified area for all possible InSAR pairs in the data set for 2018 eruption. Blue line marks day 190 (July 9 2018), the approximate date at which lava flows completely covered the active lava flow area sample region. Left: samples over an active lava flow area, specifically parts of the old 1955 lava flow that were completely covered by the 2018 Eruption. Green letters show regions of interest representing certain snapshots of lava flow evolution which are further discussed in section 4.1. Region A, represents both acquisitions taken

before the eruption, B one acquisition taken before and one after, C long time-span acquisitions taken after the eruption and D short time-span acquisitions taken after the eruption respectively. Right: samples over inactive lava flow area.

3.2 Analysis of 2022 Eruption

Figure 5 shows the average correlations of all possible C-band image pairs for both the active & inactive areas for the 2022 eruption data set. As with the 2018 eruption, there is a clear pattern of the correlation dropping and staying low after the eruption is present in the active lava flow area but not the inactive area. Bands of lowered correlation in the inactive area data are, as in the previous example, most likely caused by moisture and ordinary noise.

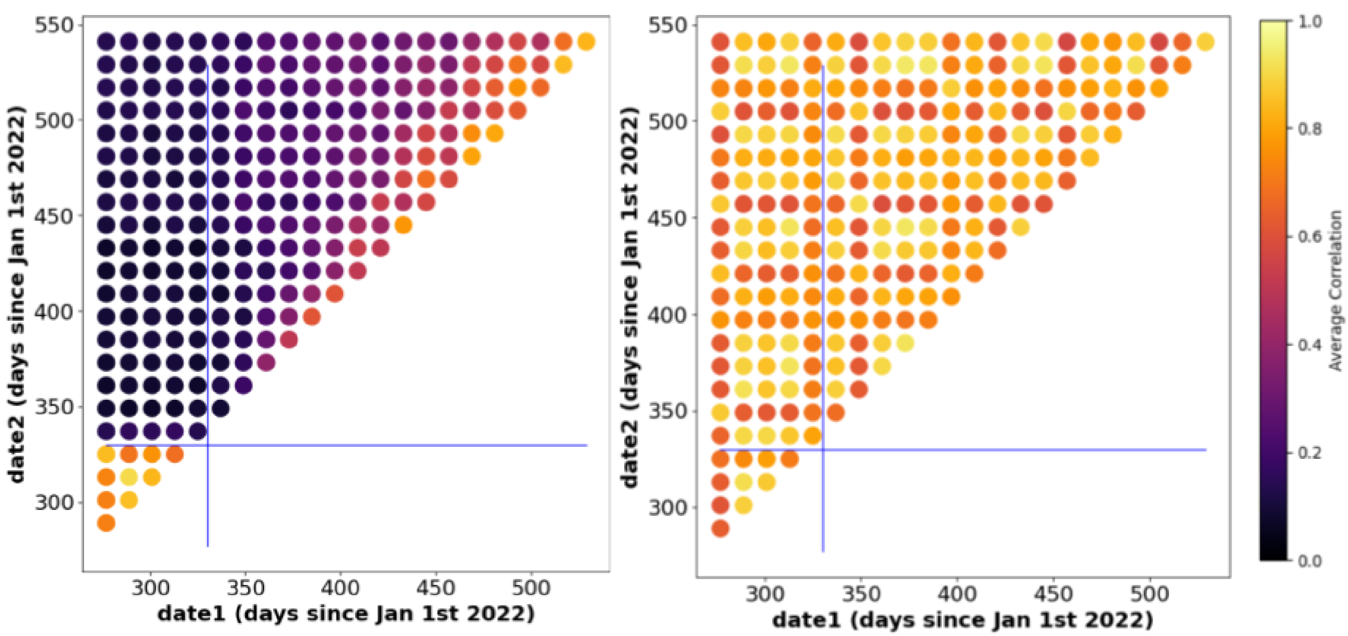

Figure 5. Plots of average correlation over active (left) and inactive (right) lava flow areas for all possible InSAR pairs in the 2022 Mauna Loa eruption data set. The blue line marks day 330 (Nov 26 2022), the approximate date at which lava flows completely covered the active lava flow area sample region.

Figure 6 shows InSAR Correlation maps of Mauna Loa made using ALOS-2 (L-band), Sentinel-1 (C-band), and CSK (X-band). All three maps were generated using images with as close to a

243 day temporal baseline as possible to simulate the aforementioned temporal baseline issues of a Venus mission. The differences between L-band and C-band are minimal, both showing the 2022 lava flow clearly. A dark halo of low coherence surrounds the summit of Mauna Loa in the L-band image, which is not volcanic in origin but results from the late December snowfall. The same snowfall signal is visible in C-band images made around the same time. X-band has significantly lower overall correlation, being far more affected by baseline effects than the other two bands. However, the new lava flows are still seen via their correlation contrast with the surrounding area.

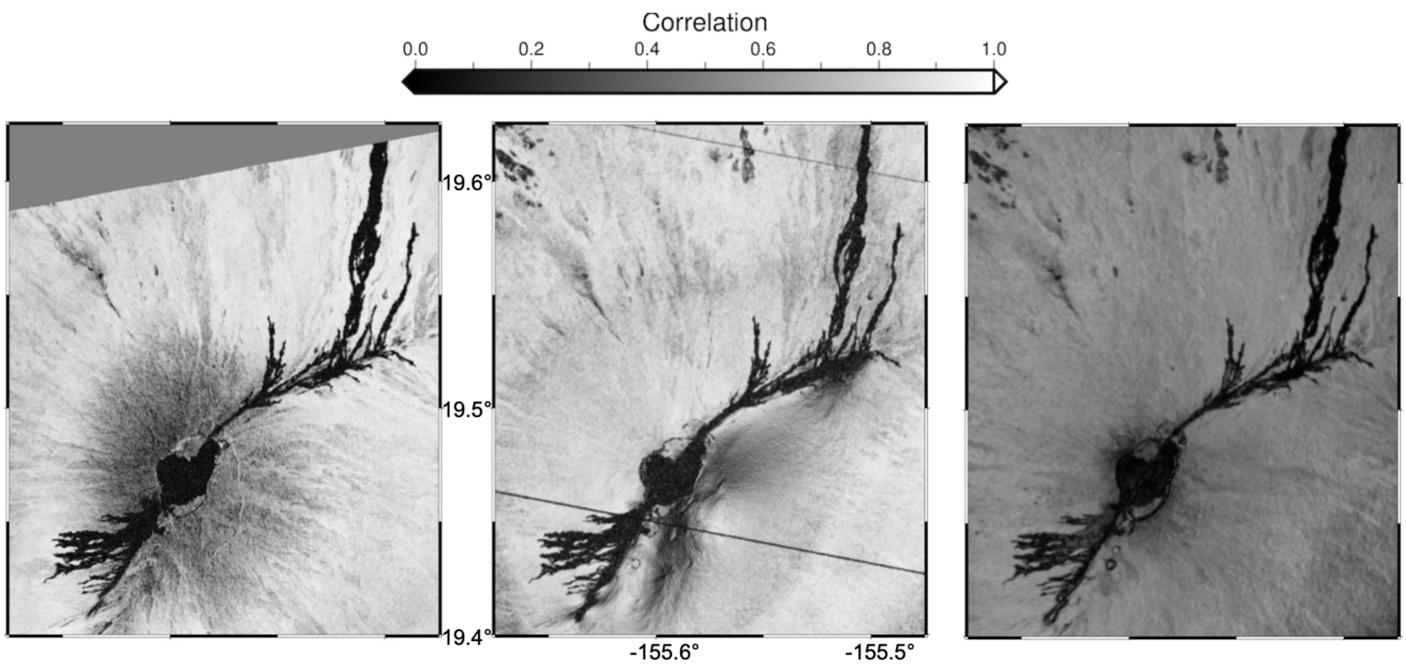

Figure 6. Left: interferogram correlation using 2 ALOS-2 L-band SAR acquisitions, one before the eruption (June 19, 2022) and one after the eruption (January 1, 2023), a temporal baseline of 196 days, the closest to 240 days possible with ALOS-2 data. Center: interferogram correlation using 2 Sentinel-1 C-band SAR acquisitions, one about 240 days before the eruption (April 8, 2022) and one during (December 4, 2022), representing 2 repeat passes of a typical Venus satellite. Straight lines going across the image mark the boundary of the Terrain Observation with Progressive Scans (TOPS) mode radar burst, and are not signals. Right: interferogram correlation using 2 CSK X-band SAR acquisitions, one during the eruption (December 2, 2022) and one after (April 25, 2023), a temporal baseline of 144 days, the closest to 240 days possible with our limited number of well correlated interferograms.

3.4 Amplitude Difference vs Correlation

Figure 7 shows the average amplitude differences of all possible image pairs for both the active and inactive areas, for both eruptions, in the C-band.

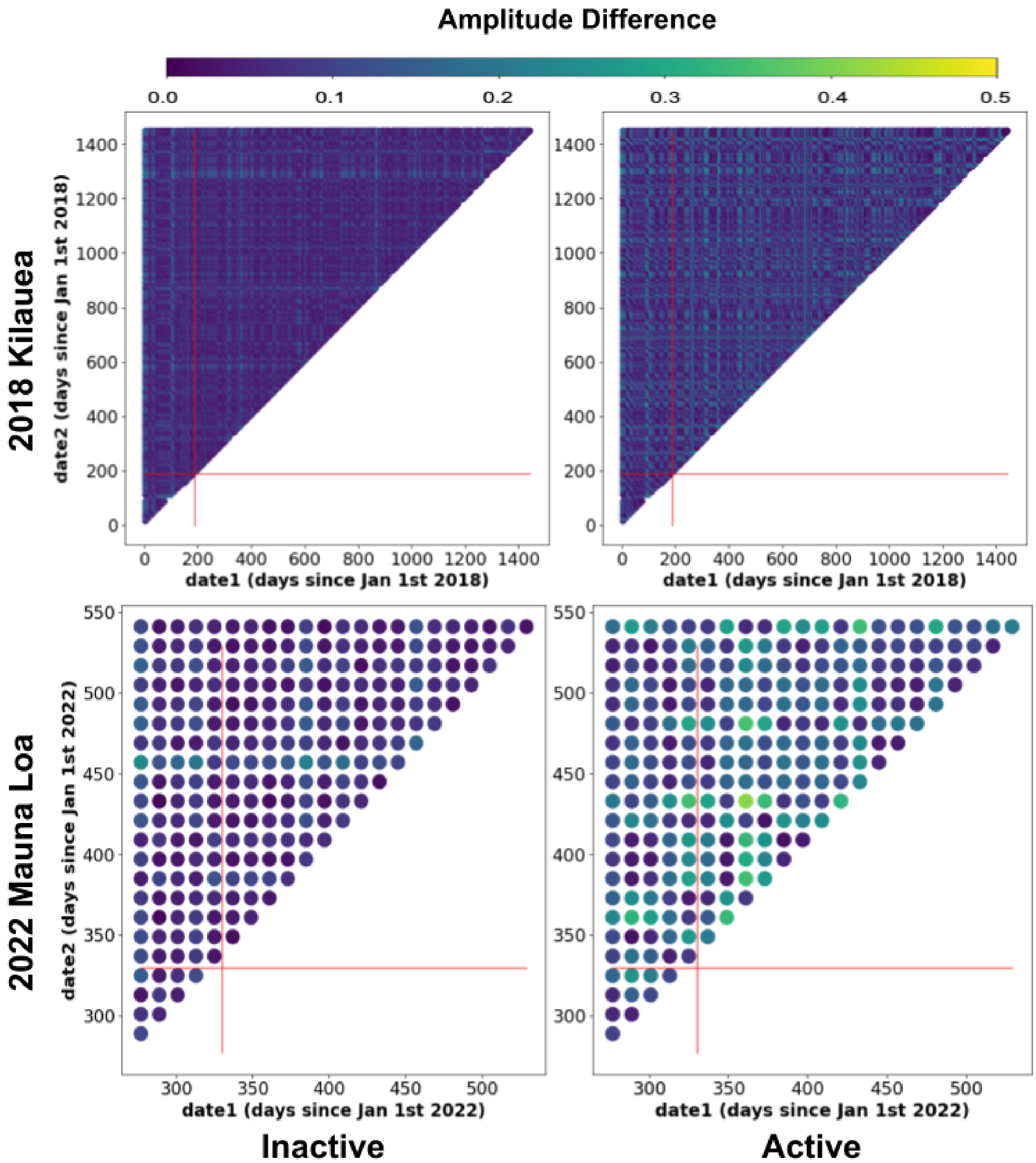

Figure 7. Plots of average SAR amplitude differences over specified areas for all possible InSAR pairs for both eruptions. Right Column: average amplitude differences of the active lava flow areas for each of two eruptions, 2018 (top) and 2022 (bottom). Left Column: average amplitude differences of the inactive lava flow areas for each of two eruptions. Red lines show the time of the volcanic event for each data set.

For the 2018 and 2022 eruption data sets, the difference between active and inactive volcanic areas is far more pronounced and temporally obvious in the average correlation data compared with the amplitude difference. In all data sets, active lava flow areas appear to have larger and more frequent changes in SAR amplitude than inactive areas. However, large amplitude differences in all three instances do not match well in time with the date of the volcanic event - it is difficult from amplitude data alone to distinguish where and when lava flow emplacement is occurring, from other events that may cause a change in backscatter (eg. precipitation). Conversely, differences in average correlation before and after a volcanic episode are immediately noticeable, and show a clear evolution in time. As is discussed in further detail in section 4.1, post-emplacement effects from the lava cooling and settling can be also clearly seen in the correlation data - something that is not visible in the amplitude difference data.

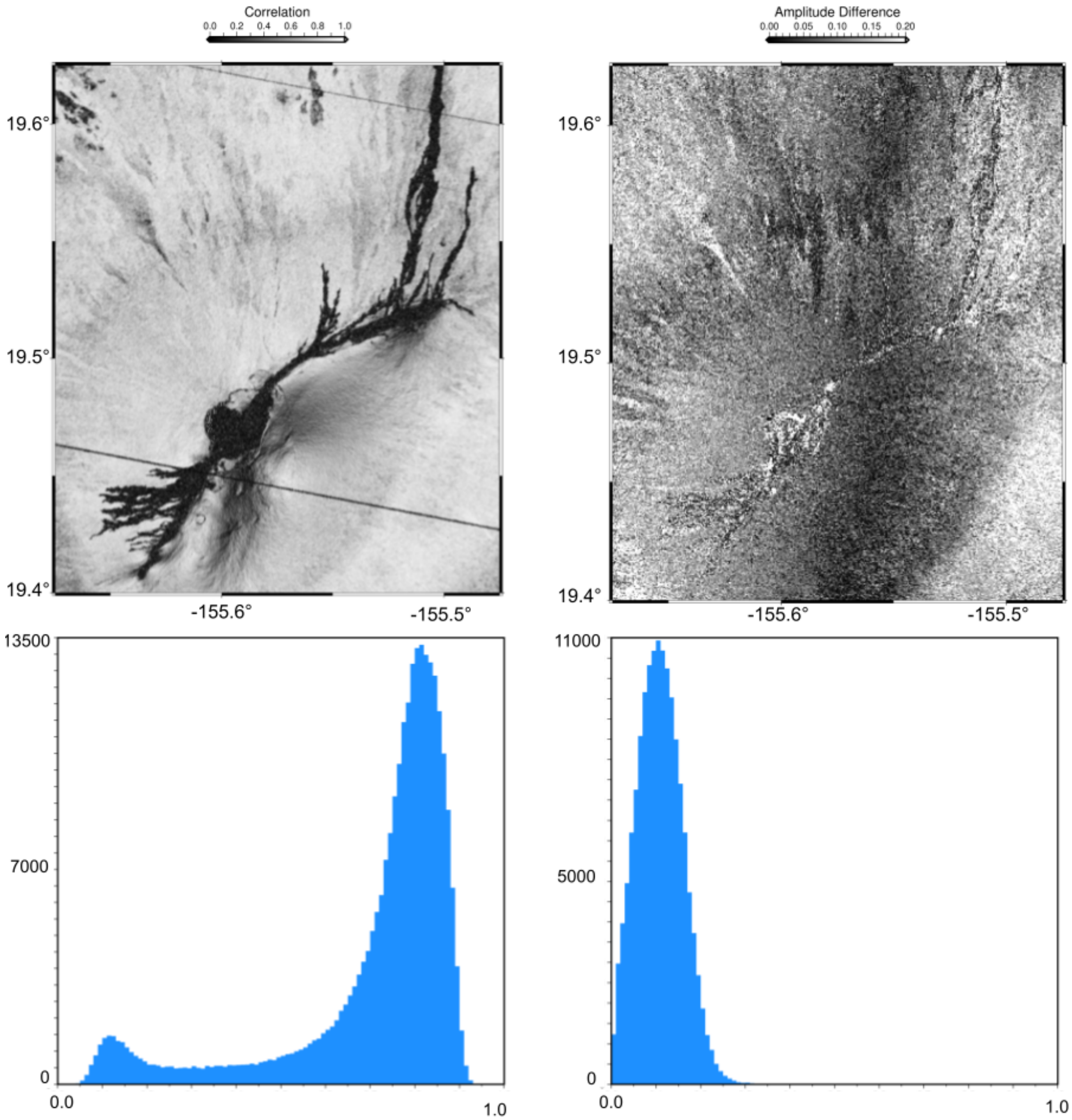

Figure 8. Top Left: interferogram correlation using 2 Sentinel-1 C-band SAR before (April 8, 2022) and during (December 4, 2022) the eruption (same as Figure 6 left), representing 2 repeat passes of a typical 243 day repeat interval at Venus. Straight lines through the image are data radar burst boundaries. Bottom Left: histogram shows the bimodal distribution of correlation. The low peak is the reduced correlation over new flows, and is smaller in amplitude because of the relatively small area of the image taken up by new flows. Top Right: absolute amplitude difference for the same pair of images, over the same geographic extent. Bottom Right: histogram shows the unimodal distribution of amplitude difference.

Figure 8 shows a map of the 2022 lava flow in both correlation and amplitude difference. In InSAR correlation data (Figure 8 top left), the decorrelated lava flow is clearly visible against the surrounding highly correlated rock. In the SAR amplitude difference data (Figure 8 top right), the lava flow is less visible, appearing similar to the surrounding surface making it more difficult to ascertain what is and is not new lava emplacement. This is reflected in the histogram distributions of each image. The correlation data shows a clear bimodal distribution (Figure 8 bottom left), meaning there is a sharp difference between low and high correlation areas. In comparison, the distribution of the amplitude difference data is unimodal (Figure 8 bottom right), meaning there are no sharp distinctions between different areas on the map. This amplitude also has a substantially lower signal-to-noise ratio compared to the correlation data.

4 Discussion and Conclusions

4.1 Post-Emplacement Signal in Correlation

Because InSAR correlation is not just a function of eruption time spans, it is not necessary to detect a volcanic event during its eruption. Instead, thermal effects on correlation mean that recent flows can be detected and their emplacement time constrained long after the event that created them. As discussed in Diettrich et al. (2012), there is a temporal delay in the recovery of high coherence. Similar delay signatures, seen in the phase of interferograms following eruptions in Iceland were attributed to cooling and thermal contraction of the lava (Wittmann et al., 2017). These post-emplacement effects are visible in Figure 4 and Figure 5. Here, even image pairs for which both images are taken after the volcanic event have a drop in correlation that does not appear in the data for the inactive area.

For both image acquisitions post-emplacement, an interferogram taken over a new lava flow will have high correlation over short time intervals, but over longer time intervals the correlation will rapidly decrease because of the instability of the subsiding surface (see the correlation change from region D to C, Figure 4 left). However, the longer a lava flow has been emplaced, the higher the stability of the surface, and therefore the smaller the resulting drop in correlation over time. This can be seen along the diagonal (Figure 4, left, region D), where interferograms are initially highly correlated before dropping off with time (Figure 4 left, region C), but the magnitude and rate of the drop decreases the further the date of the first acquisition is from the date of the eruption.

Figure 9 shows the evolution in time of the InSAR correlation of the 2022 Mauna Loa lava flow. The correlation gradually recovers over time as the lava settles and cools. Even when capturing both pre- and post-eruption acquisitions a couple of months later, the distinct outline of the lava flow remains clearly visible, exhibiting lower correlation compared to the surrounding rock (Figure 9 right). The northern, thicker and more distal part of the flow also continues to have consistently lower correlation (Figure 9).

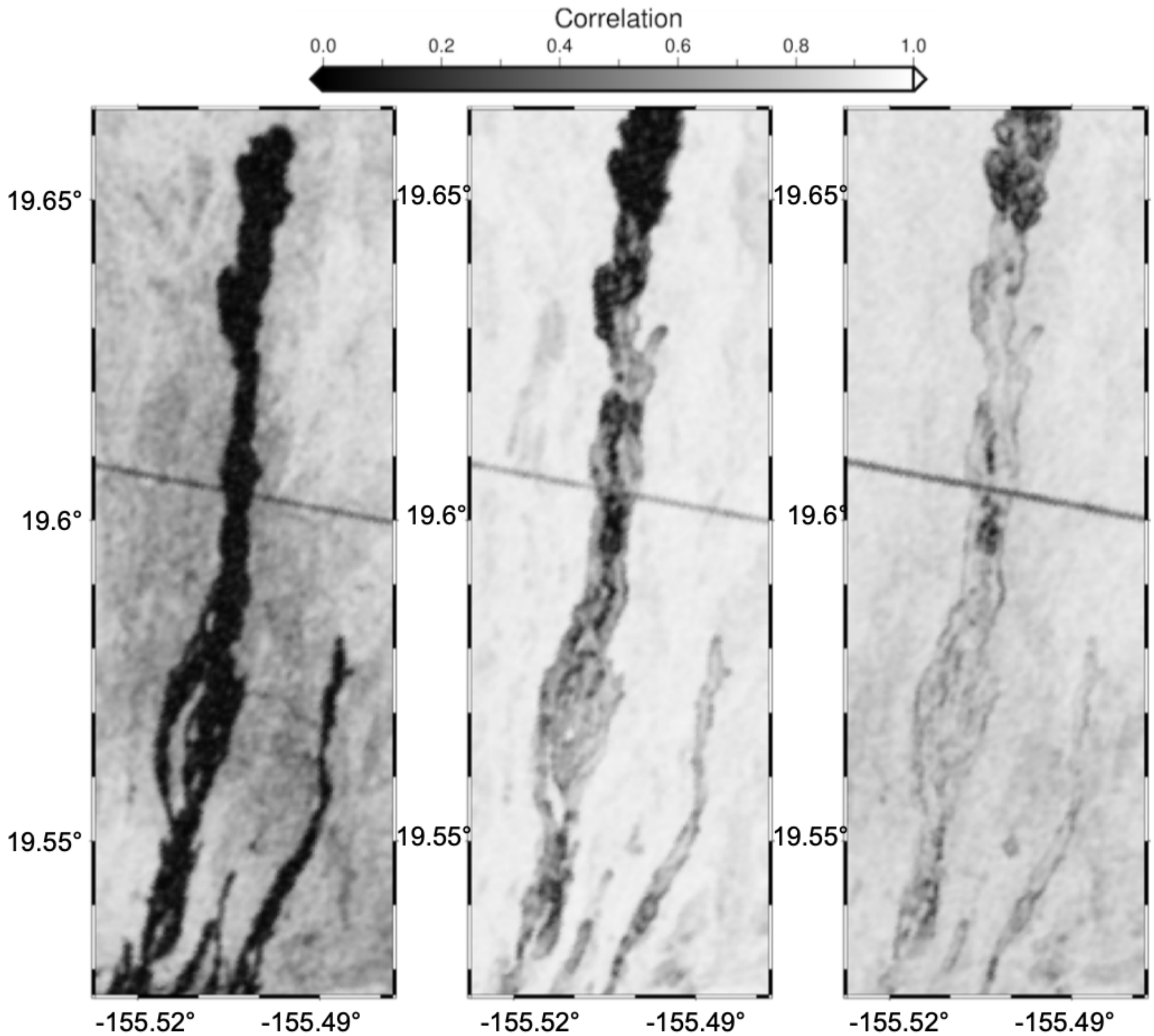

Figure 9. Time evolution of InSAR correlation over 2022 lava flow. Left: InSAR correlation map of Mauna Loa lava flow using two Sentinel-1 C-band SAR acquisitions, November 21 through December 3, 2022. Center: InSAR Correlation map of the same area, December 27, 2022 through January 8, 2023. Right: InSAR Correlation map of the same area, February 1 through February 12, 2023. Lines through each image mark the boundary of the TOPS mode radar burst and are not signals.

If both SAR acquisitions are taken before the eruption, the correlation of the resulting interferogram will be very high (see region A, Figure 4 left). If one acquisition is taken before the eruption and the other acquisition taken any time after the eruption, the InSAR correlation will be very low (see Figure 3, Figure 4 left region B, and Figure 9 left). If the first acquisition is taken relatively shortly after the eruption and second acquisition taken long after, then the resulting InSAR correlation will be low, though higher than the previous scenario (see region C, Figure 4 left, and Figure 9 center). If both the first and second acquisitions are taken long after the eruption, then the correlation will be higher as the new lava flow becomes more and more stable. Long time scale cooling effects on correlation would only be seen if the time between acquisitions was great, but short temporal baselines would show high correlation (see region D, Figure 4 left).

It is therefore important to know how quickly a lava flow settles and stops having any effect on InSAR correlation. How long a lava flow takes to become stable is dependent on its thickness, its rate of thermal subsidence, and the wavelength of the radar band detecting the change. Whittmann et al. (2017) used InSAR phase to detect an exponential decay time in the thermal subsidence of 4-6 years following eruptions in Iceland having a thickness of 8-30 m. The thickness of the 2022 Mauna Loa flow is similar, ranging from 5-25 m and up to 40 m in some areas (NASA Earth Observatory 2022), meaning the thermal subsidence time of this flow should be similar.

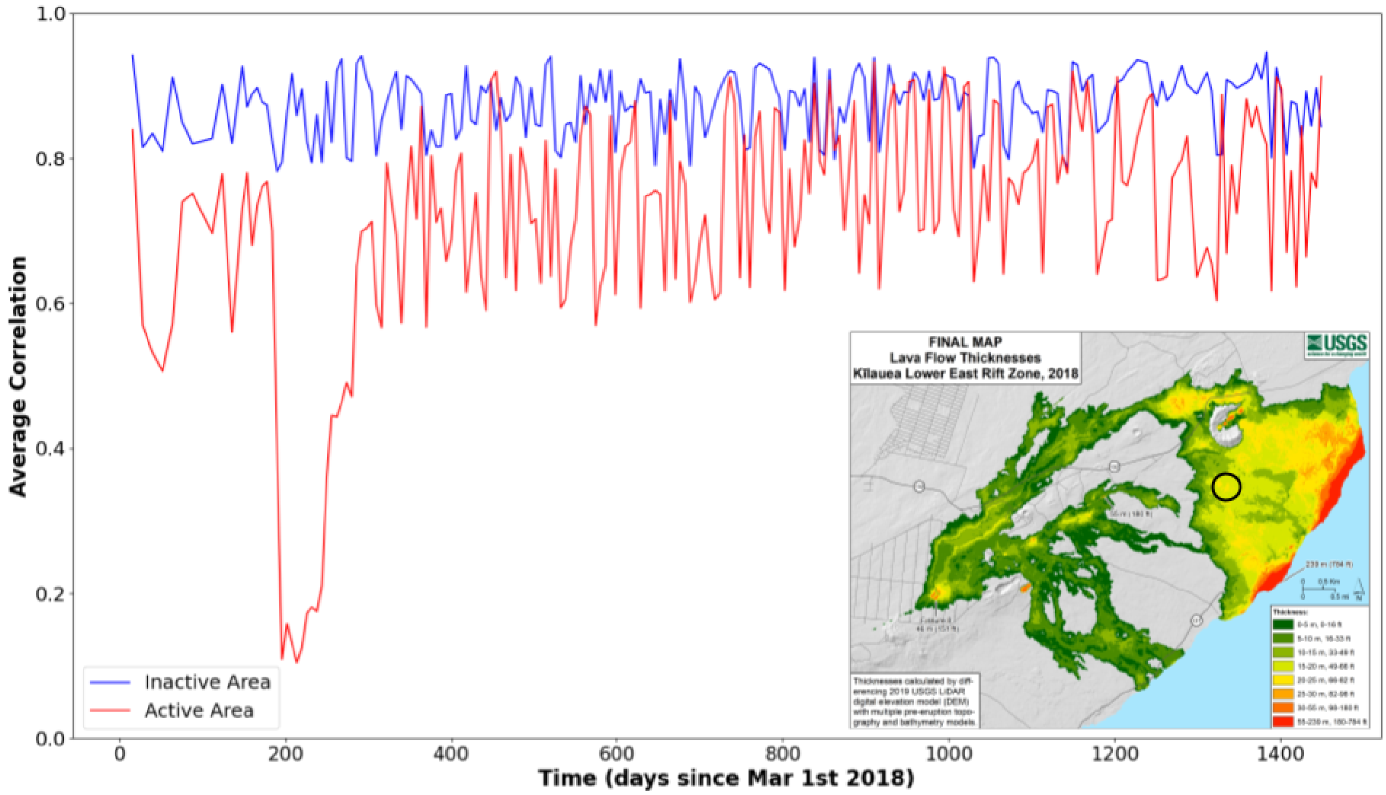

Figure 10. Average InSAR correlation for sequential interferograms over active (red) and inactive (blue) lava flow areas, between sequential images in the 2018 data set (C-band), showing the evolution in time of correlation in both areas. Lava emplacement occurred around day 190 (July 9, 2018). Inset: USGS lava flow thickness map for the 2018 eruption (USGS, 2020). Black circle shows the general location of the active lava flow area.

As shown by Diettrich et al. (2012), there is a linear relation between the length of time an emplaced lava flow is decorrelated in sequential InSAR data, and the lava thickness. This relation is also dependent upon the band of radar used - the post-emplacement change in coherence differs among wavelengths because of their different sensitivities to phase change rates caused by the settling of the flow. Though the results of Diettrich et al. (2012) were done using L-band, our own C-band results from the 2018 eruption fit broadly well with their linear model. Our active lava flow area for the 2018 eruption had a lava flow thickness of around 10-15 m and took around 175-200 days to recover sequential InSAR correlation (Figure 10). This duration of decorrelation vs lava flow thickness value is the same as that predicted by the model of Diettrich et al. (2012).

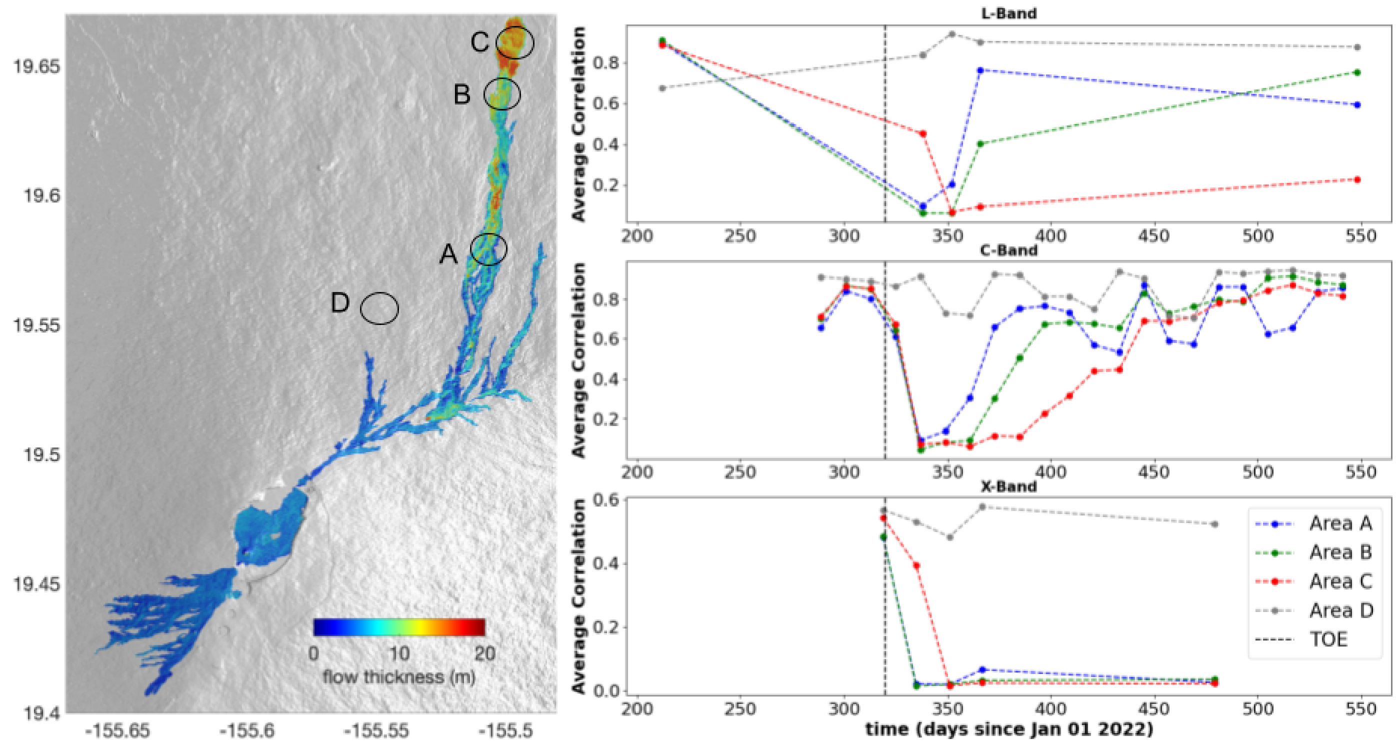

Figure 11: Evolution of average correlation of sequential interferograms over multiple areas of the 2022 Mauna Loa eruption event for 3 different bands. Lava emplacement around day 330. Left: lava flow thickness map for the 2022 Mauna Loa eruption (NASA/JPL, 2022). Lava flow thickness map generated using UAVSAR and TanDEM-X (Lundgren, Bagnardi, & Dietterich, 2019). Circles A, B, C, and D represent sample areas, each with different flow thicknesses: 10, 15, 20, and 0 (no lava) meters respectively. Right: Average correlation vs time for areas A, B, C, and D from (top) ALOS-2 data L-band , (center) Sentinel-1 data C-band, and (bottom) CSK data X-band data. The cyan line on all 3 subplots represents the time of emplacement (TOE).

Figure 11 shows the evolution of correlation of sequential interferograms versus time for various lava thicknesses for each radar band. Slight, episodic decreases in correlation can be seen, particularly in the C-band area D sample data, which are most likely due to noise and not weather, as area D is too far from the summit of Mauna Loa to be covered by snowfall. For all lava thicknesses, longer wavelengths have shorter durations of decorrelation. X-band decorrelation signatures possibly remain for longer than at L-band or C-band, however it is difficult to state this for certain due to the paucity of X-band data. L-band has the shortest decorrelation duration, at just ~30 days for Area A. This is due to the same phase changes corresponding to smaller line-of-sight ground motions. As expected, for all bands, increased lava thickness leads to longer duration of decorrelation, as the thicker the lava flow is, the longer it takes to cool and settle. This is most notable in the C-band, where area A exhibited high correlation after ~50 days, area B after ~75 days, and area C did not achieve high correlation until ~150 days post-emplacement.

4.2 Relevance to Future Venus Missions

Our results from Hawai'i indicate that InSAR correlation is more informative than SAR amplitude differences for detecting and mapping lava flows, because differences in correlation can more readily distinguish between volcanically active and inactive surfaces. The occurrence of a new lava flow will have a far larger effect on correlation than on amplitude because any new lava flow changes the random scattering properties of the surface and will cause a change in InSAR coherence. Amplitude difference primarily detects changes in the overall statistical roughness properties of the surface, which stay largely the same for similar types of lava flows. Furthermore, on Earth, InSAR correlation also allows the detection of post emplacement signals, which can last several months or even years depending on lava flow thickness and radar wavelength, as discussed in section 4.1.

The following considerations are critical to a future Venus mission. First, any relevant scenarios from our analyses of data over Hawai'i must fit with the necessarily large temporal baselines. Second, use of InSAR correlation for lava flow detection on Earth is most effective in arid areas and the application to Venus requires consideration of any environmental factors that could decrease coherence on the Venus surface, especially over time scales on the order of several months to years. Third, identification of volcanic activity via detection of post-emplacement signals is dependent on the cooling and subsidence rate of new flows, that in turn depend on surface conditions, the likely thicknesses of lava flows, and the radar wavelength used (Section

4.1). Finally, physical baselines and decorrelation from atmospheric disturbances need to be considered in future InSAR studies at Venus. We discuss each of these considerations below.

As noted in the introduction, same-look, repeat-pass SAR acquisitions at Venus will be separated in time by at least ~240 days, 1 Venus sidereal day. Therefore for Venus, one should not expect to detect any scenarios that require observations taken within a short temporal baseline (e.g., see region D, Figure 4 left and Figure 9). If the first SAR acquisition is around the time of an eruption, then the second SAR acquisition will be at minimum several months post emplacement. The resulting interferogram would have low correlation within the lava flow, and higher correlation outside the lava flow.

Changes in the radar properties of the Venus surface relevant to InSAR analyses could also result from changes in the cm-scale morphology of flows (fresh or ancient) that in turn occur because of chemical weathering or wind erosion (e.g. Herrick et al., 2023), and/or changes in radar emissivity from surface-atmosphere chemical interactions. The latter have been known since early during the Magellan mission to occur over the limited surface area of the planet at altitudes corresponding to planetary radii greater than ~6054 km (e.g. Pettengill et al., 1992; Schaeffer and Fegley, 2004). More generally, chemical reactions that could occur anywhere on the planet and affect radar emissivity or cm-scale roughness are the topic of considerable recent analog experimental and theoretical work (e.g. Dyar et al., 2021; Filiberto et al., 2020; Santos et al., 2023). These studies are motivated by the implications of weathering for identification of major compositional units (felsic versus mafic) and weathering state (fresh versus weathered) across the planetary surface via near-IR emissivity (e.g. Smrekar et al., 2010). The timescales over which chemical weathering occurs are currently unclear and estimates range from a few hours (Filiberto et al., 2020), to days (Santos et al., 2023) to up to 0.5 Ma to affect a ~30 micron-thick surface layer (Dyar et al., 2021). From a radar perspective however, these time scales are either much shorter (Filiberto et al., 2020; Santos et al., 2023) or much longer (Dyar et al., 2021) than the ~240 day interval between SAR acquisitions. If we consider a fresh flow superimposed on an older flow, short time scale reactions would not affect the old (presumably already somewhat altered) flow, but change the fresh flow almost instantly after emplacement but have little overall subsequent effect. Radar detection of a post-emplacement signal over time scales of hundreds of days would then be dominated by thermal considerations rather than chemical weathering. From a pragmatic perspective, both VERITAS and EnVision will carry spectrometers that will measure near-IR emissivity. Detection of less-weathered (hence potentially active) regions via such measurements (e.g. Dyar et al., 2023) could help identify high priority targets for InSAR studies.

Venusian surface conditions, namely the much higher ambient temperature and different atmospheric conductive properties, mean that Venusian lava flows will cool and settle at different rates than they do on Earth. According to Snyder (2002), lava on the surface of Venus takes 30-40% longer to cool than on Earth, because of the thermal convective properties of CO_2 in Venus' atmosphere, assuming similar lava composition and initial temperature. Considering this, a lava flow similar to the 2022 Mauna Loa eruption occurring on Venus would continue to thermally subside for 5-8 years post emplacement. The actual thicknesses of lava flows on Venus are uncertain, but are unlikely to be substantially thinner than on Earth. Using the model of Diettrich et al. (2012), as well as our own analysis, along with the results of Snyder (2002), we predict that a lava flow on Venus similar to the 2022 Mauna Loa eruption, with a thickness of 5-40 m, would remain decorrelated in InSAR for 160-650 days post-eruption depending on thickness, in the L-band at least, and significantly longer in the X-band. This remains only a rough estimate, since the surface temperature on Venus is much higher than on Earth. This means that even if VERITAS' first SAR acquisition is not made until 1.5-2 Earth years after an eruption, an eruption similar to the Mauna Loa 2022 lava flow may still be visible in InSAR correlation data. InSAR correlation thus also allows for the detection of post emplacement signals which can last several months or even years depending on lava flow thickness, and radar wavelength.

The use of InSAR correlation to detect new flows during or post-emplacement does not appear limited by radar wavelength, as pronounced decorrelation appears in all three bands we tested. Shorter bands have the benefit of post-emplacement signals lasting longer, while longer bands have the benefit of higher overall correlation. ESA's EnVision, although not currently planned to perform InSAR, possesses a radar that is InSAR capable. This SAR instrument will utilize S-band (9.4 cm), between the C-band and L-band tested in this paper (ESA/SCI, 2021). NASA's

VERITAS, which is planned to perform some InSAR, will be on the boundary between X and C bands (3.8 cm) and be more similar to terrestrial C-band satellites in terms of performance (Smrekar et al., 2022).

As expected, large physical perpendicular baselines remain the largest hurdle in a potential Venus InSAR mission. Large physical perpendicular baselines have a far larger effect on InSAR correlation than temporal baselines, making the highly elliptical orbit of a Venus mission a greater challenge than the long time spans between repeat acquisitions. Distinguishing between uncorrelated, new lava flows and correlated, old inactive surfaces is more difficult when the overall correlation threshold is lowered by large baselines. X-band in particular is very sensitive to this issue, as smaller wavelengths lead to smaller critical baselines. An example of a poorly correlated X-band interferogram can be seen in Figure 12.

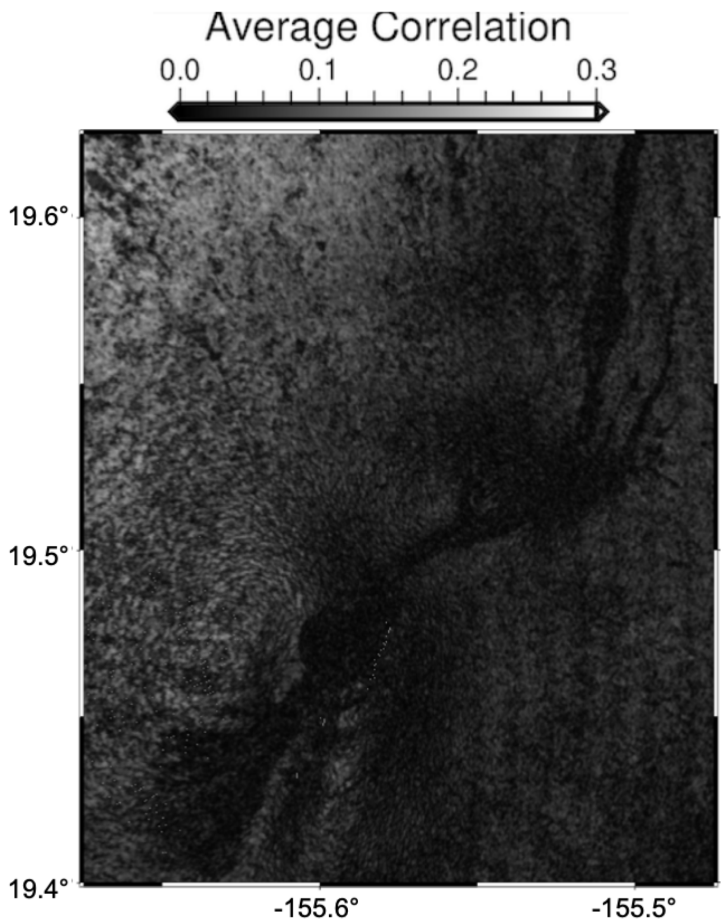

Figure 12: interferogram correlation using 2 CSK X-band SAR acquisitions, focused on the summit of Mauna Loa. First image acquisition on October 14, 2022, second image acquisition on January 18, 2023, with a perpendicular baseline of around 747 m.

Even though the image is poorly correlated, evidence of new lava flows emplaced on older lava flows can still be seen, though it is difficult to distinguish from baseline-related noise. Still, even one repeat pass with a reasonable perpendicular baseline would allow for the detection of newly emplaced lava flows, and potentially the age and thickness of flows. VERITAS, and, depending on the final reconstructed spacecraft trajectories, EnVision could potentially perform repeat pass SAR observations with moderately low physical perpendicular baselines over a few select regions of the Venusian surface, allowing for InSAR correlation analysis of such areas (Hensley et al., 2022; ESA/SCI, 2023).

There is a benefit to using longer wavelength radars for InSAR, as longer wavelengths have longer critical baselines, allowing InSAR to be done at higher physical perpendicular baselines, which lessens the need for precise orbit control. As high physical perpendicular baseline to critical baseline ratios have a detrimental effect on InSAR correlation, we believe that longer radar wavelengths are optimal for our lava detection method. Longer radar wavelengths also travel more easily through Venus' atmosphere, reducing the impact of attenuation on the signal to noise of the correlation signal (Duan et al., 2010; Meyer & Sandwell, 2012). A higher radar bandwidth also linearly increases the length of the critical baseline, however higher bandwidth radar produces a higher volume of data, requiring the satellite to have a faster data downlink.

Finally, the thick and turbulent atmosphere of Venus may affect the InSAR phase severely (Meyer & Sandwell, 2012), creating complications to detect phase signals, for instance thermal subsidence with the method of Whittmann et al. (2017). However, as long as atmospheric phase distortions occur over length scales greater than the multilook averaging length scale (~150 m), the correlation signals would survive (Meyer & Sandwell, 2012). Alternatively, if the atmospheric phase distortions occur over length scales less than the multilook averaging length scale, coherence will be diminished.

The potential use of InSAR correlation to detect and track lava flows on Venus should be given more attention. The recent discovery of modern-day volcanic activity on Venus (Herrich & Hensley, 2023) comes at a time of renewed scientific interest in Earth's sister planet, with VERITAS and EnVision planned to perform detailed SAR imaging of Venus in the next decades. InSAR, although not a priority for these upcoming missions, can provide indisputable evidence for volcanic activity because, as we have shown, InSAR correlation can be used to accurately detect and map these lava flows, even with only post-emplacement data acquisitions.

Data Availability Statement

Sentinel-1 image and orbital data was accessed via the ESA's Copernicus Open Data Hub via the Alaska Satellite Facility Vertex Data Search (ASF/ESA, 2022). CSK data was accessed from the Hawai'i Volcanoes Supresite via the ESA Geohazard Exploration Platform (GEO-GNSL, 2023). ALOS-2 data was accessed via an individual proposal to JAXA (JAXA, 2022), and was the only dataset we used in this paper which is not open access. Our DEM was generated using the SRTM1 model, as accessed through the GMTSAR website's DEM generator (Sandwell & Xiaohua, 2022).

Acknowledgements

MB and DS were supported by the NASA Earth Surface and Interior program under grants 80NSSC19K1043 and 80NSSC23K0744. CLJ and MBR acknowledge support from the NASA EnVision VenSAR Science Team program. We would like to thank Hannah Diettrich for her help in accessing lava flow thickness data and Xiahou Xu for his help with GMTSAR technical issues. We thank Richard Ghail, Mike Poland, and Paul Lundgren for comments that greatly improved the manuscript.

References

Anderson, F. S., & Smrekar, S. E. (2006). Global mapping of crustal and litho-spheric thickness on venus. Journal of Geophysical Research: Planets, 111(E8). Retrieved from https://agupubs.onlinelibrary.wiley.com/doi/abs/ 10.1029/2004JE002395 doi: https://doi.org/10.1029/2004JE002395

ASF/ESA. (2022). Copernicus sentinel data, retrieved from ASF DAAC. Retrieved from https://asf.alaska.edu

Brossier, J., Gilmore, M. S., Toner, K., & Stein, A. J. (2021). Distinct mineralogy and age of individual lava flows in Atla Regio, Venus derived from magellan radar emissivity. Journal of Geophysical Research: Planets , 126 (3), e2020JE006722. Retrieved from https://agupubs.onlinelibrary.wiley .com/doi/abs/10.1029/2020JE006722 (e2020JE006722 2020JE006722) doi: https://doi.org/10.1029/2020JE006722

Byrne, P. K., Ghail, R. C., S ̧engo ̈r, A. C., James, P. B., Klimczak, C., & Solomon, S. C. (2021). A globally fragmented and mobile lithosphere on venus. Proceed- ings of the National Academy of Sciences, 118(26), e2025919118.

Byrne, P. K., & Krishnamoorthy, S. (2022). Estimates on the frequency of volcanic eruptions on venus. Journal of Geophysical Research: Planets, 127(1), e2021JE007040. Retrieved from https://agupubs.onlinelibrary.wiley.com/doi/abs/10.1029/2021JE007040 (e2021JE007040 2021JE007040) doi: https://doi.org/10.1029/2021JE007040

Campbell, B. A. (1999). Surface formation rates and impact crater densities on venus. Journal of Geophysical Research: Planets, 104(E9), 21951-21955. Retrieved from https://agupubs.onlinelibrary.wiley.com/doi/abs/ 10.1029/1998JE000607 doi: https://doi.org/10.1029/1998JE000607

Darby, D.M., Helbert, J., Cooper, R.F., Sklute, E.C., Maturilli, A., Mueller, N.T., Kappel, D., Smrekar, S.E., Surface weathering on Venus: Constraints from kinetic, spectroscopic, and geochemical data, Icarus, Volume 358, 2021, 114139, ISSN 0019-1035, https://doi.org/10.1016/j.icarus.2020.114139. (https://www.sciencedirect.com/science/article/pii/S0019103520304802)

Dietterich, H. R., Poland, M. P., Schmidt, D. A., Cashman, K. V., Sherrod, D. R., & Espinosa, A. T. (2012). Tracking lava flow emplacement on the east rift zone of K ̄ılauea, Hawai‘i, with synthetic aperture radar coherence. Geochemistry, Geophysics, Geosystems, 13 (5). Retrieved from https://agupubs.onlinelibrary.wiley.com/doi/abs/10.1029/2011GC004016 doi: https://doi.org/10.1029/2011GC004016

Dietterich, H.R., Diefenbach, A.K., Soule, S.A. *et al.* Lava effusion rate evolution and erupted volume during the 2018 Kīlauea lower East Rift Zone eruption. *Bull Volcanol* **83**, 25 (2021). https://doi.org/10.1007/s00445-021-01443-6

D'Incecco, P., Mu ̈ller, N., Helbert, J., & D'Amore, M. (2017). Idunn Mons on Venus: Location and extent of recently active lava flows. Planetary and Space Science, 136, 25-33. Retrieved from https://www.sciencedirect.com/ science/article/pii/S003206331630112X doi: https://doi.org/10.1016/ j.pss.2016.12.002

Dualeh, E. W. (2022, September). Potential of synthetic aperture radar backscatter for monitoring volcanic eruptions. Retrieved from https://etheses.whiterose.ac.uk/31768/

Dualeh, E. W., Ebmeier, S. K., Wright, T. J., Albino, F., Naismith, A., Biggs, J., . . . Roca, A. (2021). Analyzing explosive volcanic deposits from satellite-based radar backscatter, Volc ́an de Fuego, 2018. Journal of Geophysical Research: Solid Earth , 126 (9), e2021JB022250. Retrieved from https://agupubs.onlinelibrary.wiley.com/doi/abs/10.1029/2021JB022250(e2021JB022250 2021JB022250) doi: https://doi.org/10.1029/2021JB022250

X. Duan, M. Moghaddam, D. Wenkert, R. L. Jordan and S. E. Smrekar, "X band and model of Venus atmosphere permittivity," in *Radio Science*, vol. 45, no. 02, pp. 1-19, April 2010, doi: 10.1029/2009RS004169. keywords: {Atmospheric modeling;Venus;Atmospheric measurements;Permittivity;Polarization;Dielectric constant},

ESA/SCI. (2021). EnVision assessment study report (yellowbook). , 127, 1-111. Retrieved from https://sci.esa.int/s/WepGERw

ESA/SCI. (2023). EnVision definition study report (redbook). , 1-175. Retrieved from https://www.cosmos.esa.int/web/envision/links

Esposito, L. W. (1984). Sulfur dioxide: Episodic injection shows evidence for active venus volcanism. Science , 223 (4640), 1072-1074. Retrieved from https://www.science.org/doi/abs/10.1126/science.223.4640.1072 doi: 10.1126/ science.223.4640.1072

Farr, T. G., Rosen, P. A., Caro, E., Crippen, R., Duren, R., Hensley, S., . . . Alsdorf, D. (2007). The shuttle radar topography mission. Reviews of Geophysics, 45 (2). Retrieved from https://agupubs.onlinelibrary.wiley.com/doi/ abs/10.1029/2005RG000183 doi: https://doi.org/10.1029/2005RG000183

Filiberto, J., Trang, D., Treiman, A. H., Gilmore, M.S., Present-day volcanism on Venus as evidenced from weathering rates of olivine. *Sci. Adv.***6**, eaax 7445(2020).DOI:10.1126/sciadv.aax7445

Gatelli, F., Monti Guamieri, A., Parizzi, F., Pasquali, P., Prati, C., & Rocca, F. (1994). The wavenumber shift in sar interferometry. IEEE Transactions on Geoscience and Remote Sensing, 32(4), 855-865. doi: 10.1109/36.298013

GEO-GSNL (2023). Hawaiian Volcanoes Supersite. Retrieved from http://geo-gsnl.org/supersites/permanent-supersites/hawaiian-volcanoes-supersite/

Ghail, R., Wilson, C., Widemann, T., Bruzzone, L., Dumoulin, C., Helbert, J., . . . Burtz, L.-J. (2017). EnVision: understanding why our most earth-like neighbor is so different.

Hauck II, S. A., Phillips, R. J., & Price, M. H. (1998). Venus: Crater distribution and plains resurfacing models. Journal of Geophysical Research: Planets, 103(E6), 13635-13642. Retrieved from https://agupubs.onlinelibrary .wiley.com/doi/abs/10.1029/98JE00400 doi: https://doi.org/10.1029/ 98JE00400

Head, J. W., Crumpler, L. S., Aubele, J. C., Guest, J. E., & Saunders, R. S. (1992). Venus volcanism: Classification of volcanic features and structures, associations, and global distribution from magellan data. Journal of Geophysical Research: Planets, 97(E8), 13153-13197. Retrieved from https://agupubs.onlinelibrary.wiley.com/doi/abs/10.1029/92JE01273 doi: https://doi.org/10.1029/92JE01273

Hensley, S., *et al*., "Planned Differential Interferometric SAR Observations at Venus by the VERITAS Mission," *IGARSS 2022 - 2022 IEEE International Geoscience and Remote Sensing Symposium*, Kuala Lumpur, Malaysia, 2022, pp. 12-15, doi: 10.1109/IGARSS46834.2022.9884339.

Herrick, R. R., Bjonnes, E. T., Carter, L. M., Gerya, T., Ghail, R. C., Gillmann, C.,. . . others (2023). Resurfacing history and volcanic activity of venus. Space Science Reviews, 219(4), 29.

Herrick, R. R., & Hensley, S. (2023). Surface changes observed on a venusian volcano during the magellan mission. Science, 379(6638), 1205-1208. Retrieved from https://www.science.org/doi/abs/10.1126/science.abm7735 doi: 10.1126/science.abm7735

JAXA. (2022). Advanced land observing satellite-2 "DAICHI-2" (ALOS-2) research and application project. Data retrieved from G-Portal https://gportal.jaxa.jp/gpr/search?tab=1

Johnson, C. L., & Sandwell, D. T. (1994, 11). Lithospheric flexure on Venus. Geo- physical Journal International, 119(2), 627-647. Retrieved from https://doi .org/10.1111/j.1365-246X.1994.tb00146.x doi: 10.1111/j.1365-246X.1994 .tb00146.x

Lohman, R.B., Bürgi, P.M., Soil moisture effects on InSAR - A correction approach and example from a hyper-arid region, Remote Sensing of Environment, Volume 297, 2023, 113766, ISSN 0034-4257, https://doi.org/10.1016/j.rse.2023.113766. (https://www.sciencedirect.com/science/article/pii/S0034425723003176)

Lu, Z., & Freymueller, J. T. (1998). Synthetic aperture radar interferometry coherence analysis over Katmai volcano group, Alaska. Journal of Geophysical Re- search: Solid Earth, 103(B12), 29887-29894. Retrieved from https://agupubs .onlinelibrary.wiley.com/doi/abs/10.1029/98JB02410 doi: https://doi .org/10.1029/98JB02410

Lu, Z., Mann, D., Freymueller, J. T., & Meyer, D. J. (2000). Synthetic aperture radar interferometry of Okmok volcano, Alaska: Radar observations. Journal of Geophysical Research: Solid Earth, 105(B5), 10791-10806. Retrieved from https://agupubs.onlinelibrary.wiley.com/doi/abs/10.1029/ 2000JB900034 doi: https://doi.org/10.1029/2000JB900034

Lundgren, P. R., Bagnardi, M., & Dietterich, H. (2019). Topographic changes during the 2018 Kīlauea eruption from single-pass airborne InSAR. Geophysical Research Letters, 46. https://doi.org/10.1029/2019GL083501

Massonnet, D., & Rabaute, T. (1993). Radar interferometry: limits and potential. IEEE Transactions on Geoscience and Remote Sensing, 31(2), 455-464. doi: 10.1109/36.214922

McKenzie, D., Ford, P. G., Johnson, C., Parsons, B., Sandwell, D., Saunders, S., & Solomon, S. C. (1992). Features on venus generated by plate boundary processes. Journal of Geophysical Research: Planets, 97(E8), 13533-13544. Retrieved from https://agupubs.onlinelibrary.wiley.com/doi/abs/ 10.1029/92JE01350 doi: https://doi.org/10.1029/92JE01350

McKinnon, W. B., Zahnle, K. J., Ivanov, B. A., & Melosh, H. (1997). Cratering on venus: Models and observations. Venus II: Geology, geophysics, atmosphere, and solar wind environment, 969.

Meyer, F. J., & Sandwell, D. T. (2012). Sar interferometry at venus for topography and change detection. Planetary and Space Science, 73(1), 130-144. Retrieved from https://www.sciencedirect.com/science/article/pii/ S0032063312002978 (Solar System science before and after Gaia) doi: https://doi.org/10.1016/j.pss.2012.10.006

Mouginis-Mark, P. (2004). Remote sensing studies of kilauea volcano, hawaii, as an aid to understanding volcanic processes on mars, venus and io. In Agu fall meeting abstracts (Vol. 2004, pp. V32A–01).

NASA Earth Observatory (2022). Sizing up mauna loa’s lava flows. Retrieved from https://earthobservatory.nasa.gov/images/150736/sizing-up-mauna-loas-lava-flows

NASA/JPL (2022). Airborne NASA Radar Maps Mauna Loa Lava Changes in Hawai‘i. Retrieved from https://www.jpl.nasa.gov/images/pia25526-airborne-nasa-radar-maps-mauna-loa-lava-changes-in-hawaii

Neal, C. A., *et al.*, The 2018 rift eruption and summit collapse of Kīlauea Volcano. *Science* 363, 367-374 (2019). DOI:10.1126/science.aav7046

Patrick, M. R., *et al.*, Cyclic lava effusion during the 2018 eruption of Kīlauea Volcano. *Science* 366, eaay9070 (2019). DOI:10.1126/science.aay9070

Pettengill, G. H., P. G. Ford, and R. J. Wilt (1992), Venus surface radiothermal emission as observed by Magellan, *J. Geophys. Res.*, 97(E8), 13091–13102, doi:10.1029/92JE01356.

Phillips, R. J., Raubertas, R. F., Arvidson, R. E., Sarkar, I. C., Herrick, R. R., Izenberg, N., & Grimm, R. E. (1992). Impact craters and Venus resurfacing history. Journal of Geophysical Research: Planets, 97(E10), 15923-15948. Retrieved from https://agupubs.onlinelibrary.wiley.com/doi/abs/ 10.1029/92JE01696 doi: https://doi.org/10.1029/92JE01696

Rowland, S. K., Harris, A. J., Wooster, M. J., Amelung, F., Garbeil, H., Wilson, L., & Mouginis-Mark, P. J. (2003). Volumetric characteristics of lava flows from interferometric radar and multispectral satellite data: the 1995 Fernandina and 1998 Cerro Azul eruptions in the western galapagos. Bulletin of Volcanology, 65, 311–330.

Russell, M. B., & Johnson, C. L. (2021). Evidence for a locally thinned lithosphere associated with recent volcanism at Aramaiti Corona, Venus. Journal of Geophysical Research: Planets, 126(8), e2020JE006783. Retrieved from https://agupubs.onlinelibrary.wiley.com/doi/abs/10.1029/2020JE006783 (e2020JE006783 2020JE006783) doi: https://doi.org/10.1029/2020JE006783

Sandwell, D., Mellors, R., Tong, X., Wei, M., & Wessel, P. (2011). GMTSAR: An InSAR processing system based on generic mapping tools.

Sandwell, D. S., Xiaohua, X., & Guns, K. (2022). Topex satellite geodesy. Retrieved from https://topex.ucsd.edu

Santos, A. R., Gilmore, M. S., Greenwood, J. P., Nakley, L. M., Phillips, K., Kremic, T., & Lopez, X. (2023). Experimental weathering of rocks and minerals at Venus conditions in the Glenn Extreme Environments Rig (GEER). *Journal of Geophysical Research: Planets*, 128, e2022JE007423. https://doi.org/10.1029/2022JE007423

Saunders, R. S., Spear, A. J., Allin, P. C., Austin, R. S., Berman, A. L., Chandlee, R. C., . . . Wall, S. D. (1992). Magellan mission summary. Journal of Geophysical Research: Planets, 97(E8), 13067-13090. Retrieved from https://agupubs.onlinelibrary.wiley.com/doi/abs/10.1029/92JE01397 doi: https://doi.org/10.1029/92JE01397

Schaber, G. G., Strom, R. G., Moore, H. J., Soderblom, L. A., Kirk, R. L., Chadwick, D. J., . . . Russell, J. (1992). Geology and distribution of impact craters on venus: What are they telling us? Journal of Geophysical Research: Planets , 97 (E8), 13257-13301. Retrieved from https:// agupubs.onlinelibrary.wiley.com/doi/abs/10.1029/92JE01246 doi: https://doi.org/10.1029/92JE01246

Schaefer, L., Fegley, B., Heavy metal frost on Venus, Icarus, Volume 168, Issue 1, 2004, Pages 215-219, ISSN 0019-1035, https://doi.org/10.1016/j.icarus.2003.11.023. https://www.sciencedirect.com/science/article/pii/S0019103503004020

Schubert, G., & Sandwell, D. (1995). A global survey of possible subduction sites on venus. Icarus, 117(1), 173-196. Retrieved from https://www.sciencedirect.com/science/article/pii/S0019103585711505 doi: https://doi.org/10.1006/icar.1995.1150

Shalygin, E. V., Markiewicz, W. J., Basilevsky, A. T., Titov, D. V., Ignatiev, N. I., & Head, J. W. (2015). Active volcanism on venus in the ganiki chasma rift zone. Geophysical Research Letters, 42(12), 4762-4769. Retrieved from https://agupubs.onlinelibrary.wiley.com/doi/abs/10.1002/ 2015GL064088 doi: https://doi.org/10.1002/2015GL064088

Sleep, N. H. (1992). Hotspot volcanism and mantle plumes. Annual Review of Earth and Planetary Sciences, 20(1), 19–43.

Smrekar, S., Hensley, S., Nybakken, R., Wallace, M. S., Perkovic-Martin, D., You, T.-H., . . . Mazarico, E. (2022). VERITAS (venus emissivity, radio science, InSAR, topography, and spectroscopy): A discovery mission. , 1-20. doi: 10.1109/AERO53065.2022.9843269

Smrekar, S. E., Ostberg, C., & O'Rourke, J. G. (2023). Earth-like lithospheric thick- ness and heat flow on Venus consistent with active rifting. Nature Geoscience, 16(1), 13–18.

Smrekar, S. E., Stofan, E. R., Mueller, N., Treiman, A., Elkins-Tanton, L., Helbert, J., . . . Drossart, P. (2010). Recent hotspot volcanism on venus from virtis emissivity data. Science, 328(5978), 605-608. Retrieved from https://www.science.org/doi/abs/10.1126/science.1186785 doi: 10.1126/science.1186785

Solomon, S. C., & Head, J. W. (1982). Mechanisms for lithospheric heat transport on venus: Implications for tectonic style and volcanism. Journal of Geophysical Research: Solid Earth, 87(B11), 9236–9246.

Stevens, N. F., Wadge, G., Williams, C. A., Morley, J. G., Muller, J.-P., Murray, J. B., & Upton, M. (2001). Surface movements of emplaced lava flows measured by synthetic aperture radar interferometry. Journal of Geophysical Research: Solid Earth , 106 (B6), 11293-11313. Retrieved from https:// agupubs.onlinelibrary.wiley.com/doi/abs/10.1029/2000JB900425 doi: https://doi.org/10.1029/2000JB900425

USGS. (Date Unknown). The Island of Hawai'i with lava flows erupted in approximately the past 1,000 years shown in red. Located on the southeastern side, Kīlauea Volcano is 90% covered with young flows. Retrieved from https://www.usgs.gov/media/images/island-hawai-i-lava-flows-erupted-approximately

USGS. (2011). July 2007 eruption - flow field map. Retrieved from https://www.usgs.gov/node/278436

USGS. (2018). map of kilauea volcano's lower east rift zone. Retrieved from https://www.usgs.gov/media/images/map-kilauea-volcanos-lower-east-rift-zone

USGS. (2020). November 23, 2020 - kilauea 2018 lower east rift zone lava flow thicknesses. Retrieved from https://www.usgs.gov/node/278815

USGS. (2022). December 4, 2022 - mauna loa eruption map. Retrieved from https://www.usgs.gov/maps/december-4-2022-mauna-loa-eruption-map

Turcotte, D. L. (1995). How does venus lose heat? Journal of Geophysical Research: Planets, 100(E8), 16931–16940.

Wittmann, W., Sigmundsson, F., Dumont, S., & Lavall´ee, Y. (2017). Post- emplacement cooling and contraction of lava flows: InSAR observations and a thermal model for lava fields at hekla volcano, iceland. Journal of Geo- physical Research: Solid Earth , 122 (2), 946-965. Retrieved from https:// agupubs.onlinelibrary.wiley.com/doi/abs/10.1002/2016JB013444 doi: https://doi.org/10.1002/2016JB013444

Zebker, H. A., Rosen, P., Hensley, S., & Mouginis-Mark, P. J. (1996, 06). Analysis of active lava flows on Kilauea volcano, Hawaii, using sir-c radar correlation measurements. Geology, 24(6), 495-498. Retrieved from https://doi.org/10.1130/0091-7613(1996)024<0495:AOALFO>2.3.CO;2 doi: 10.1130/0091-7613(1996)024⟨0495:AOALFO⟩2.3.CO;2

Zebker, H. A., Villasenor, J., et al. (1992). Decorrelation in interferometric radar echoes. IEEE Transactions on geoscience and remote sensing, 30(5), 950–959.